Atomlike interaction and optically tunable giant band-gap renormalization in large-area atomically thin math xmlns="http://www.w3.org/1998/Math/MathML">msub>mi >MoS/mi>mn>2/mn>/msub>/math>

Santu K. Bera, Megha Shrivastava, Khamari Bramhachari, Hanyu Zhang, Ajay K. Poonia, Dipendranath Mandal, E. M. Miller, Matthew C. Beard, Amit Agarwal, and K. V. Adarsh

Atom like interaction and optically tunable giant bandgap renormalization in large area atomically thin MoS$_2$

Santu K. Bera,[1] Megha Shrivastava,[1] Khamari Bramhachari,[2] Hanyu Zhang,[3] Ajay K. Poonia,[1] Dipendranath Mandal,[1] E.M. Miller,[3] Matthew C. Beard,[3] Amit Agarwal,[2, *] and K. V. Adarsh[1, †]

[1]*Department of Physics, Indian Institute of Science Education and Research Bhopal, Bhopal 462066, India*
[2]*Department of Physics, Indian Institute of Technology, Kanpur 208016, India*
[3]*Chemistry and Nanoscience Science Center, National Renewable Energy Laboratory, Golden, Colorado 80401, USA*

Coulomb interactions in atomically thin transition metal dichalcogenides can be dynamically engineered by exploiting the dielectric environment to control the optical and electronic properties. Here, we demonstrate an optically tunable giant bandgap renormalization (BGR) $\sim$ 1200 and 850 meV from the edge of the conduction band and complete suppression of the exciton absorption in large-area single-layer (1L) and three-layer (3L) MoS$_2$, respectively. The observed giant BGR is two orders of magnitude larger than that in the conventional semiconductors, and it persists for 10s of ps. Strikingly, our results demonstrate photoinduced transparency at the electronic bandgap using an intense optical field at room temperature. Exciton bleach recovery in 1L and 3L show a contrasting fluence dependent response, demonstrating the layer dependent optical tuning of exciton lifetime in a way that would be both reversible and real-time. We find that the optical bandgap (exciton resonance peak) shows a transient redshift followed by an anomalous blueshift from the lowest energy point as a function of the photo-generated carrier density. The observed exciton energy shift is analogous to atom-atom interactions, and it varies as a Lennard-Jones like potential as a function of the inter-exciton separation.

Atomically thin transition metal dichalcogenides (TMDCs) are a new class of two-dimensional (2D) semiconductors that have enabled the study of quantum confined materials in the ultimate thickness limit of one or a few unit cells [1–3]. In the 2D limit, due to reduced dielectric screening and quantum confinement, the effective strength of the Coulomb interactions is enhanced. As a consequence, the optical response is dominated by strongly bound excitons and other excitonic complexes [4–12]. The strong unscreened Coulomb interaction in conjugation with quantum many-body effects plays a central role in determining the optical (E_x) and electronic (E_g) bandgaps in TMDCs. TMDCs offer a new approach for unprecedented tunability of the optical and electronic properties by engineering the dielectric environment and inducing changes in the screening of the Coulomb interactions [13–16]. Experimentally, this can be achieved using different methods like chemical doping [17], electrostatic gating [15, 18], applying external magnetic field [19] and mechanical strain [20, 21], among others. However, such methods are usually perturbative and not suitable for continuous tuning of the electronic and optical bandgaps by a large amount.

Coulomb engineering by optical carrier injection via intense ultrashort laser pulses offers an alternative nonperturbative approach, for realizing the full potential of TMDCs in photonic and optoelectronic applications. For example, earlier work on mechanically exfoliated TMDCs under intense photoexcitation has shown a large bandgap renormalization (BGR) of up to 500 meV [22]. However, most studies on BGR have focussed only on the modification of the optical bandgap while ignoring the renormalization of the spectrum beyond the electronic bandgap regime (in the range of 2.4−2.9 eV) [23–26] in TMDCs [22, 27–29]. Furthermore, most previous studies were performed for low pump fluence values, which are either below or in the vicinity of the Mott density. In this regime, the impact of the applied optical field can be treated as a single-photon effect neglecting the contribution of the multi-photon and other higher order contributions [15, 29–32]. In fact, the BGR and other interesting physical phenomena occurring for fluences above the Mott-density regime are yet to be explored and understood. Likewise, the role of layer-dependent multicarrier effects, including Auger recombination and phonon bottleneck in direct bandgap single-layer (1L) and indirect bandgap three-layer (3L) MoS$_2$, largely remains unclear.

In this Letter, we demonstrate an all-optically tunable giant BGR of nearly 1200 (850) meV from the electronic bandgap and complete suppression of exciton absorption in both the large area grown 1L (3L) MoS$_2$, when the applied photon fluence is beyond the Mott density. The unusually broad differential absorption (DA) spectrum includes strong photoinduced absorption from the electronic conduction band edge to 300 meV below the optical bandgap and induced transparency in the electronic bandgap region due to spectral shift. Further, the 3L MoS$_2$ shows a significantly longer exciton lifetime, up to a 2-fold increase over the lifetime observed in 1L MoS$_2$ at higher fluence, demonstrating the possibility of layer dependent optical tuning of the exciton lifetime. Moreover, the optical bandgap shows a tran-
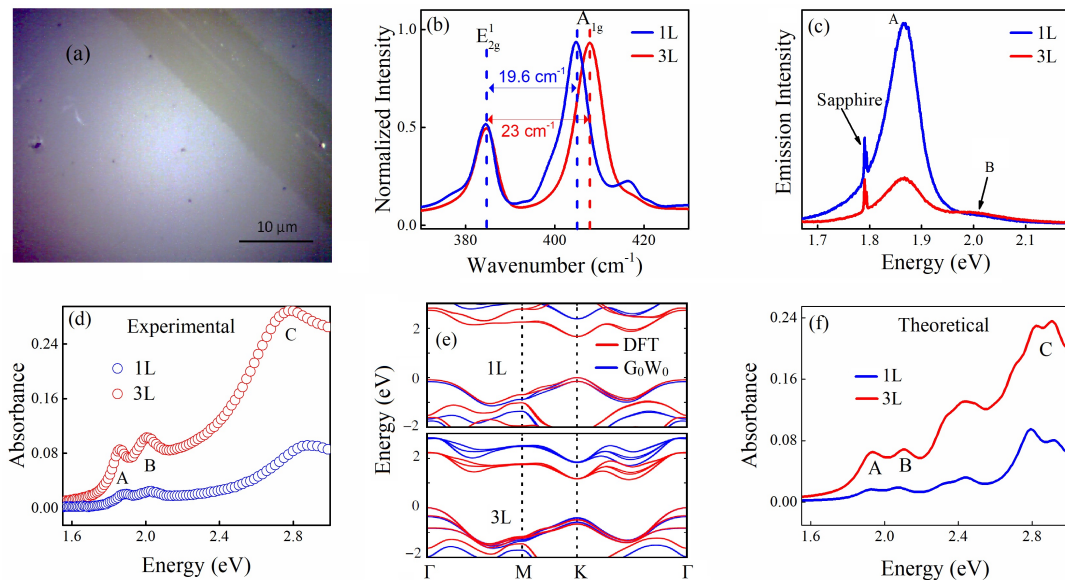
FIG. 1. Optical microscopic image of CVD grown 1L MoS$_2$ on sapphire crystal shows uniformity in the large scale. (b) Raman spectra and (c) PL spectra of 1L (blue) and 3L (red) MoS$_2$. (d) Ground state optical absorption of 1L (blue) and 3L (red) MoS$_2$. (e) Electronic band structure calculated using G$_0$W$_0$ (blue) and DFT (red). (f) Absorption spectrum obtained by solving BSE for 1L (blue) and 3L (red) MoS$_2$.

sient redshift followed by an anomalous blueshift with increasing density of the photo-generated carriers. On plotting the observed exciton energy shift as a function of the inter-exciton distance, we find that it mimics the Lennard-Jones like potential for atom-atom interactions. This demonstrates that in the low exciton density regime, the exciton physics is governed by the exciton-exciton attraction and charge carrier screening physics, while the repulsive exciton-exciton interactions govern the high exciton density regime.

Our wafer-scale continuous and oriented 1L and 3L MoS$_2$ films were grown on the sapphire crystal by chemical vapor deposition using a three-temperature-zone furnace (for details, see Supplemental Material [33]). The optical microscopy image in Fig. 1(a) shows that the film is continuous over a large area without any cracks or islands. The Raman spectra presented in Fig. 1(b) show two characteristic E_{2g}^1 and A_{1g} modes, and the separation between these modes (19.6 and 23 cm^{-1}) qualitatively confirms that our two samples contain 1L and 3L [34–36]. The μ-PL spectra of 1L and 3L shown in Fig. 1(c) demonstrate emissions from the A and B excitons. The 3-fold reduction in PL intensity of 3L compared to 1L shows their indirect bandgap nature. The Raman and PL mapping shown in Fig. S1 [33] additionally confirms the high quality and large area continuity of our samples.

Figure 1(d) shows the optical absorption of the 1L (3L) MoS$_2$ and it clearly resolves the three characteristic excitons: A at 1.88 ± 0.01 eV (1.85 ± 0.01 eV), B at 2.02 ± 0.01 eV (2.00 ± 0.01 eV), and C at 2.87 ± 0.01 eV (2.76 ± 0.01 eV), consistent with previous reports [37–

39]. Compared to the bulk spectrum, the sharpness and peak positions of the A and B excitons highlight the reduced dielectric screening in the 2D limit [1, 9, 11]. The first two lower-energy excitons originate from the doubly degenerate valence band formed of Mo atoms at the K point in the Brillouin zone, and the energy separation between them highlights the strong spin-orbit coupling [40]. The quasiparticle band structure calculated using the G$_0$W$_0$ and density functional theory (DFT) are shown in Fig. 1(e) (See [33] for details of the calculation) [41–44, 46, 47]. The corresponding absorption spectra obtained by solving the Bethe-Salpeter equation (BSE) are shown in Fig. 1(f), consistent with our experiments.

Going beyond the equilibrium regime, we now explore how the photoexcited charge carriers modulate the excitons of atomically thin TMDCs at room temperature and tune the electronic and optical bandgaps along with the exciton binding energy [27, 28, 48]. To this end, we perform fluence dependent ultrafast DA spectroscopy measurements (for details see the SM [33]). The samples were excited with 100 fs pump pulses of photon energy 1.94 eV, tuned just above the A exciton energy (1.88 eV). The change in the absorbance (ΔA) of the excited state is probed by broadband white light pulses (1.5 to 3 eV) covering a wide spectrum. The color-coded fluence dependent DA spectra are shown in Fig. 2(a) for 1L and in Fig. 2(b) for 3L MoS$_2$. It highlights the dramatic modification of the optical response by means of the photo doping of the charge carriers. Our experimental results above the Mott density regime clearly establish i) the complete suppression of the absorption feature in the A and B ex-
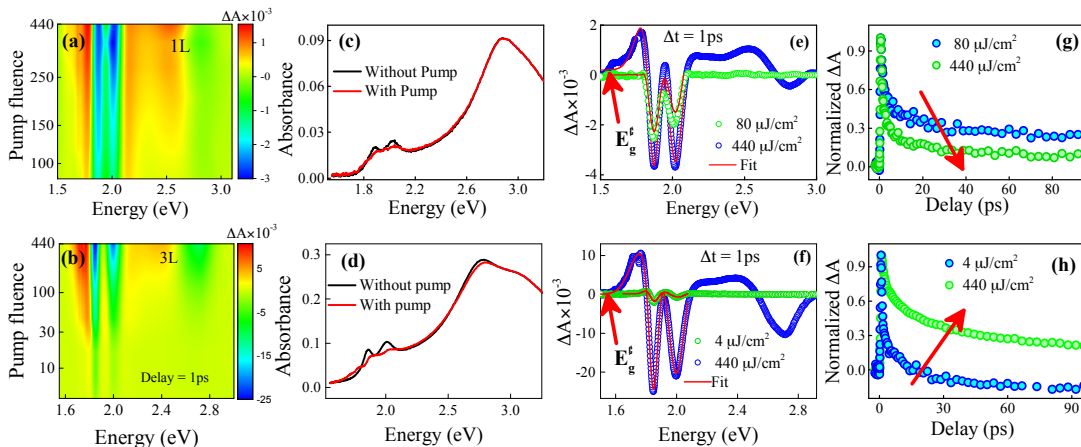
FIG. 2. FIG. 2. Color-coded DA spectrum as a function of carrier density showing drastic spectral change above Mott density for (a) 1L and (b) 3L MoS$_2$. The absorbance spectra without (black) and with (red) pump showing the complete suppression of A and B exciton resonance at 440 μJ/cm^2 for (c) 1L and (d) 3L MoS$_2$. Spectral view of DA for two extreme fluences at pump-probe delay 1 ps for (e) 1L and (f) 3L MoS$_2$. Decay kinetics of A exciton for two extreme fluences (only two extreme fluence data is shown for clarity) of (g) 1L and (h) 3L MoS$_2$.

citon resonances [Figs. 2(c) and 2(d)], ii) the emergence of novel photoinduced absorption from the edge of the electronic bandgap to $\sim$300 meV below A exciton resonance energy and iii) photoinduced transparency in the electronic bandgap region above 2.74 eV (2.40 eV) for 1L (3L) MoS$_2$ due to spectral shift.

To better understand the nature of BGR, we examine the DA spectra for two extreme fluences, as shown in Fig. 2(e) for 1L and Fig. 2(f) for 3L. The DA spectral features at low pump fluence can be described as a combination of bleach at the A and B exciton energies (due to phase-space filling) and photoinduced absorption sidebands (due to exciton line-broadening). Interestingly, the DA spectrum is completely flat above the B exciton energy. With the increase in excitation fluence, the densities of the excitons increase gradually, and beyond the Mott density, the excitons are converted into electron-hole plasma. This leads to the complete disappearance of the main excitonic resonances shown in Figs. 2(c) and 2(d), which can also be visualized from the saturation of bleach with increasing fluence in Fig. S3 [33].

The critical photoexcited carrier density (n) at which the exciton resonance vanishes is called the Mott-density (n_{Mott}). We estimate it to be $n_{\text{Mott}} \sim 10^{13}$ cm^{-2} using the relation $a_0 n_{\text{Mott}}^{1/2} = 0.25$ for 2D, where a_0 is the exciton radius [49]. Similar value of n_{Mott} is also theoretically estimated in previous report [12]. For $n > n_{\text{Mott}}$, the large population of the free carriers in the electron-hole plasma screen the Coulomb potential, which in combination with the fermionic exchange and correlation effects lead to the dramatic modification in the band structure [25, 50]. Overall, this results in the drastic changes in the DA spectrum [see Fig. 2(e)], particularly in the energy range between the electronic bandgap, $E_g \sim 2.74$ eV[23–

25] and the new renormalized bandgap $E_g^{'} \sim 1.52$ eV, marked in Fig. 2(e) by onset (lower energy end) of wide induced absorption due to electron-hole plasma. This amounts to a giant BGR $\sim$ 1200 meV in 1L MoS$_2$. Similarly, we observe the BGR value for 3L MoS$_2$ to be 860 meV with $E_g \sim$2.4 eV [51] and $E_g^{'} \sim$1.54 eV [see Fig. 2(f)]. This observation of giant BGR in 1L MoS$_2$ is two orders of magnitude larger than the observed value in conventional semiconductors in highly screened environments [22, 51–54]. Between 1L and 3L, the observed BGR value in 1L is nearly 1.5 times than 3L MoS$_2$. The reported BGR values for different semiconductors with respect to our present observation are listed in Table SI of the SM [33]. Additionally, we observed ultrafast photoinduced transparency right above the conduction band edge at room temperature, arising from the spectral shift. We explicitly checked that even at these high pump fluences, the measurements were reproducible, and there was no sample damage or any structural phase-transition due to excitation.

At this point, it is essential to confirm that the broad photoinduced absorption feature for $E < E_g$ arises from BGR since this energy region can also host trions and biexcitons (or other exciton complexes) [7, 32]. To separate the contributions from BGR and other correlated bound state effects, we have analyzed the kinetic traces of the induced absorption above the Mott density, in Fig. S4 of the SM [33], for 1L and 3L MoS$_2$ at two selected energies, 1.73 and 2.26 eV. The kinetic traces at 1.73 eV possess a fast decay at an early time scale, and then it merges with the kinetic trace for 2.26 eV with increasing time, after which both the features decay simultaneously. The fast decay component ($\sim$10%) can possibly be attributed to trions forming $\sim$20 meV below the A exciton

energy [32]. The simultaneous decay at two different absorption regions indicate that they indeed have a common origin, which is BGR.The observed changes in spectroscopic properties with optical pumping are qualitatively similar in 1L and 3L MoS$_2$, but they show significant variations in their magnitude.

To better understand the underlying photophysical properties of the exciton lifetime, we compare the decay kinetics of the A exciton for 1L and 3L as a function of excitation fluence in Figs. 2(g) and 2(h). Remarkably, we find a contrasting behavior in the bleach recovery of A exciton in 1L and 3L MoS$_2$ with increasing fluence. For instance, the bleach recovery dramatically slows down in 3L, whereas it becomes faster in 1L with increasing fluence. The fast bleach recovery in 1L MoS$_2$ occurs due to the exciton-exciton annihilation/Auger recombination [55], manifesting strong many-body interactions. We attribute the comparatively slow bleach recovery of 3L MoS$_2$ with increasing fluence to the phonon bottleneck arising from its indirect bandgap[33], in addition to defect assisted recombination [56]. To confirm that the exciton lifetime in 3L is phonon mediated, we compare the exciton bleach recovery of 3L MoS$_2$ at room and liquid nitrogen temperature (77K). Indeed, we observe a slow exciton bleach recovery at 77 K in 3L MoS$_2$ (see Fig. S6 in SM [33]). This highlights that the exciton lifetime is at least two times longer in 3L as compared to 1L. Additionally, it establishes the important result that the exciton-exciton annihilation/Auger recombination in 3L (with an indirect bandgap) is suppressed in comparison with 1L MoS$_2$ (with a direct bandgap).

To corroborate our experimental findings, we calculated the fluence dependence of the observed optical spectrum using the real time evolution of the Bethe-Salpeter equation (BSE)[42, 57]. The calculated fluence dependent absorption spectra for 1L MoS$_2$ are shown in Fig. 3(a). The black arrow highlights the redshift of the A exciton peak with increasing pump fluence. We also find a decrease in the absorption peak amplitude with increased pump fluence, indicating the bleaching of the exciton peaks.

After demonstrating the giant BGR in the electronic bandgap, and establishing the suppression of Auger recombination in 3L MoS$_2$, we focus on the change in the optical bandgap induced by the photoexcited carrier density. For this, we monitored the optical bandgap as a function of the pump fluence, and the spectral shifts were obtained by the global fitting of the DA for the A and B excitons (see [33]). The shift of the A exciton energy as a function of the fluence is shown in Fig. 3(b). We find that with increasing excitation fluence, the optical bandgap shows a gradual redshift and reaches the maximum value ∼72 (120) meV for 300 μJ/cm^2 in 1L (3L) MoS$_2$. This redshift can be attributed to the BGR arising from the presence of excited charge carriers, as discussed earlier. Interestingly, Fig. 3(b) shows redshift
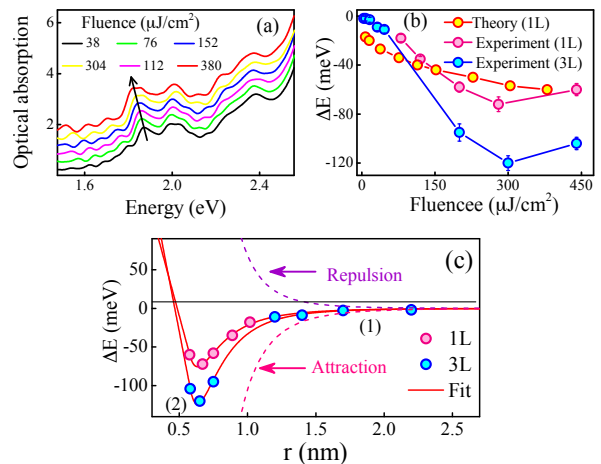

FIG. 3. (a) Calculated optical absorption spectrum for different values of the pump fluence. The black to red line coreesponds to the fluence value from 38 to 380 μJ/cm^2, and the different curves are shifted vertically for clarity. The black arrow highlights the redshift of the A exciton peak with increasing pump fluence. (b) Shift in A exciton resonance calculated from theory (1L) and experiment (1L and 3L) (c) Shift of exciton energy with variation of average exciton distance with the fitting by Lennard-Jones like potential with modified exponent (red solid curve).

value is smaller in 1L compared to 3L. This is because of the larger reduction in the binding energy due to a larger carrier screening in 1L compared to 3L. The theoretically calculated fluence dependent change in the A exciton energy is shown in Fig. 3(b) for 1L MoS$_2$. Our calculations, which include the effect of carrier-excitons interactions, qualitatively capture the observed redshift of the A exciton energy with increasing pump fluence.

On increasing the carrier denisty further, we observed an anomalous blueshift of 13 (16) meV for 1L (3L) from the maximum redshifted value. However, the real time simulations of BSE do not capture the blueshift at higher fluences. This is expected, as the BSE calculations do not include the repulsive exciton-exciton interactions[58]. To understand this anomalous blue-shift in the high carrier density regime (with small inter-exciton separation), we model the exciton-exciton interactions via a Lennard-Jones like potential, in a manner similar to the case of atom-atom interactions. Accordingly, the exciton energy shift has the following form,

$$\Delta E = A\left[\left(\frac{r_0}{r}\right)^p - \left(\frac{r_0}{r}\right)^q\right] . \tag{1}$$

Here, r is the average distance between the excitons, which is related to the photoexcited carrier density (n) by $n\pi r^2 = 1$. In Eq. (1), r_0, p, and q are the equilibrium distance between the excitons, repulsive exponent and attractive exponent, respectively, which we use as fitting parameters. The observed exciton energy shift (ΔE) as function of the average inter-exciton separation (r) is

shown in Fig. 3(c), and it is captured well by Eq. (1). The modified exponents for the repulsive and attractive part of the exciton-exciton interactions are found to be $p = 7.2 \pm 0.1$ (6.0 ± 0.2), $q = 4.2 \pm 0.2$ (5.3 ± 0.3), and $r_0 = 0.53 \pm 0.03$ (0.54 ± 0.01) nm in 1L (3L) MoS$_2$. We find that the attractive exponent is higher for 3L MoS$_2$. This is consistent with the larger redshift observed in 3L compared to 1L. Clearly, in the high exciton density regime [marked as region (2) in Fig. 3(c)], the short range repulsive exciton-exciton interactions dominate, and this leads to the blueshift of the exciton energy.

In summary, we have demonstrated i) complete restructuring of the band structure in atomically thin TMDCs by optically injecting carriers above the Mott density, ii) suppression of the Auger recombination in 3L MoS$_2$, and iii) atom-like repulsive short ranged interactions in 1L and 3L MoS$_2$. The observed giant BGR ($\sim$1200 meV) is two orders larger than that reported in other conventional semiconductors. Furthermore, exciton bleach recovery shows a contrasting fluence and layer dependent response, demonstrating the possibility to optically tune the exciton lifetime in a way that would be both reversible and real-time. Additionally, by tracking the fluence dependence of the exciton energy in the Mott density regime, we show that the exciton-exciton interaction potential behaves like a Lennard-Jones potential for inter-atomic interactions. Our work paves way for controlled and reversible tunability of the optical properties of TMDs which can help unlock their full potential in optoelectronic and photonic devices.

[1] G. Wang, A. Chernikov, M. M. Glazov, T. F. Heinz, X. Marie, T. Amand, and B. Urbaszek, Rev. Mod. Phys. **90**, 021001 (2018).

[2] K. F. Mak, C. Lee, J. Hone, J. Shan, and T. F. Heinz, Phys. Rev. Lett. **105**, 136805 (2010).

[3] S. Manzeli, D. Ovchinnikov, D. Pasquier, O. V. Yazyev, and A. Kis, Nat. Rev. Mater. **2**, 17033 (2017).

[4] K. F. Mak, K. He, C. Lee, G. H. Lee, J. Hone, T. F. Heinz, and J. Shan, Nat. Mater. **12**, 207-211 (2013).

[5] A. Chernikov, T. C. Berkelbach, H. M. Hill, A. Rigosi, Y. Li, O. B. Aslan, D. R. Reichman, M. S. Hybertsen, and T. F. Heinz, Phys. Rev. Lett. **113**, 076802 (2014).

[6] H. Komsa and A. V Krasheninnikov, Phys. Rev. B 86, 241201 (2012).

[7] C. Zhang, H. Wang, W. Chan, , C. Manolatou, and F. Rana, Phys. Rev. B **89**, 205436205445 (2014).

[8] K. He, N. Kumar, L. Zhao, Z. Wang, K. F. Mak, H. Zhao, and J. Shan, Phys. Rev. Lett. **113**, 026803 (2014).

[9] D. Y. Qiu, F. H. Jornada, and S. G. Louie, Phys. Rev. Lett. **111**, 216805 (2013).

[10] E. J. Sie, A. J. Frenzel, Y. H. Lee, J. Kong, and N. Gedik, Phys. Rev. B **92**, 125417 (2015)

[11] A. Ramasubramaniam, Phys. Rev. B **86**, 115409 (2012).

[12] A. Steinhoff, M. Florian, M. Rsner, G. Schnhoff, T.O. Wehling, and F. Jahnke, Nat Commun **8**, 1166 (2017).

[13] Y. Lin, X. Ling, L. Yu, S. Huang, A. L. Hsu, Y. Lee, J. Kong, and M. S. Dresselhaus, Nano Lett. **14**, 5569-5576 (2014).

[14] A. Raja, A. Chaves, J. Yu, G. Arefe, H. M. Hill, A. F. Rigosi, T. C. Berkelbach, P. Nagler, C. Schller, T. Korn, C. Nuckolls, J. Hone, L. E. Brus, T. F. Heinz, D. R. Reichman, and A. Chernikov, Nat. Commun. **8**, 15251 (2017).

[15] A. Chernikov, A. M. Van Der Zande, H. M. Hill, A. F. Rigosi, A. Velauthapillai, J. Hone, and T. F. Heinz, Phys. Rev. Lett. **115**, 126802 (2015).

[16] I. Kylanpaa and H. Komsa, Phys. Rev. B **92**, 205418 (2015).

[17] S. Gao and L. Yang, Phys. Rev. B **96**, 155410 (2017).

[18] Z. Qiu, M. Trushin, H. Fang, I. Verzhbitskiy, S. Gao, E. Laksono, M. Yang, P. Lyu, J. Li, J. Su, M. Telychko, K. Watanabe, T. Taniguchi, J. Wu, A. H. Castro Neto, L. Yang, G. Eda, S. Adam, and J. Lu, Sci. Adv. **5**, eaaw2347 (2019).

[19] M. Goryca, J. Li, A. V. Stier, T. Taniguchi, K. Watanabe, E. Courtade, S. Shree, C. Robert, B. Urbaszek, X. Marie, and S. A. Crooker, Nat. Commun. **10**, 4172 (2019).

[20] H. J. Conley, B. Wang, J. I. Ziegler, R. F. Haglund, S. T. Pantelides, and K. I. Bolotin, Nano Lett. 13, 3626-3630 (2013).

[21] H. Shi, H. Pan, Y. W. Zhang, and B. I. Yakobson, Phys. Rev. B **87**, 155304 (2013)

[22] A. Chernikov, C. Ruppert, H. M. Hill, A. F. Rigosi, and T. F. Heinz, Nat. Photonics **9**, 466-470 (2015).

[23] T. Y. Jeong, H. Kim, S. Choi, K. Watanabe, Y. Kim, S. Jung, T. Taniguchi, and K. J. Yee, Nat. Commun **10**, 3825 (2019).

[24] L. Wang, Z. Wang, H. Y. Wang, G. Grinblat, Y. L. Huang, D. Wang, X. H. Ye, X. Bin Li, Q. Bao, A. S. Wee, S. A. Maier, Q. D. Chen, M. L. Zhong, C. W. Qiu, and H. B. Sun, Nat. Commun **8**, 13906 (2017).

[25] A. Steinhoff, M. Rsner, F. Jahnke, T. O. Wehling, and C. Gies, Nano Lett. **14**, 3743- 3748 (2014).

[26] M. M. Ugeda, A. J. Bradley, S. F. Shi, F. H. Da Jornada, Y. Zhang, D. Y. Qiu, W. Ruan, S. K. Mo, Z. Hussain, Z. X. Shen, F. Wang, S. G. Louie, and M. F. Crommie, Nat. Mater. **13**, 1091-1095 (2014).

[27] Y. Park, S. W. Han, C. C. S. Chan, B. P. L. Reid, R. A. Taylor, N. Kim, Y. Jo, H. Im and K. S. Kim, Nanoscale, **7**, 10647 (2017).

[28] H. CoyDiaz, F. Bertran, C. Chen, J. Avila, J. Rault, P. L.Fvre, M. C. Asensio, M. Batzill, Phys. Status Solidi RRL **9**, 701706 (2015)

[29] P. D. Cunningham, A. T. Hanbicki, K. M. McCreary, and B. T. Jonker, ACS Nano **11**, 12601-12608 (2017).

[30]] E. A. A. Pogna, M. Marsili, D. De Fazio, S. Dal Conte, C. Manzoni, D. Sangalli, D. Yoon, A. Lombardo, A. C. Ferrari, A. Marini, G. Cerullo, and D. Prezzi, ACS Nano **10**, 1182-1188 (2016).

[31] F. Liu, M. E. Ziffer, K. R. Hansen, J. Wang, and X. Y. Zhu, Phys. Rev. Lett. **122**, 246803 (2019).

[32] R. E. Wood, L. T. Lloyd, F. Mujid, L. Wang, M. A. Allodi, H. Gao, R. Mazuski, P. C. Ting, S. Xie, J. Park, and G. S. Engel, J. Phys. Chem. Lett. **11**, 2658-2666 (2020).

[33] See Supplemental Material for details of sample growth, Raman and PL mapping, details of theoretical calculatins, Ultrafast transient absorption (TA) spectroscopy setup, saturation of bleach intensity above Mott-density, Kinetic traces of induced absorption due to BGR, Exciton bleach recovery, renormalization of optcal bandagp, Comparison of optically induced BGR values for different semiconductors

[34] C. Lee, H. Yan, L. E. Brus, T. F. Heinz, J. Hone, and S. Ryu, ACS Nano **4**, 2695-2700 (2010).

[35] J. Jeon, S. K. Jang, S. M. Jeon, G. Yoo, Y. H. Jang, J. H. Park, and S. Lee, Nanoscale **7**, 1688-1695 (2015).

[36] B. Chakraborty, H. S. S. R. Matte, A. K. Sood, and C. N. R. Rao, J. Raman Spectrosc. **44**, 9296 (2013).

[37] Q. H. Wang, K. Kalantar-Zadeh, A. Kis, J. N. Coleman, and M. S. Strano, Nat. Nanotechnol. **7**, 699-712 (2012).

[38] K. Yao, A. Yan, S. Kahn, A. Suslu, Y. Liang, E. S. Barnard, S. Tongay, A. Zettl, N. J. Borys, and P. J. Schuck, Phys. Rev. Lett. **119**, 087401 (2017).

[39] C. Zhang, H. Wang, W. Chan, C. Manolatou, and F. Rana, Phys. Rev. B **89**, 205436 (2014).

[40] G. A. Ermolaev, Y. V. Stebunov, A. A. Vyshnevyy, D. E. Tatarkin, D. I. Yakubovsky, S. M. Novikov, D. G. Baranov, T. Shegai, A. Y. Nikitin, A. V. Arsenin, and V. S. Volkov, Npj 2D Mater. Appl.**4**, 21 (2020).

[41] P. Giannozzi, S. Barroni, N. Bonini, M. Calandra, R. Car, C. Cavazzoni, D. Ceresoli, L. C. Guido, M. Cococcioni and I. Dabo, J. Phys. Condens. Matter **21**, 395502 (2009).

[42] A. Marini, C. Hogan, M. Gruning, D. Varsano, Comput. Phys. Communication **180**, 1392-1403 (2009).

[43] G. Onida, L. Reining, and A. Rubio Rev. Mod. Phys. **74**, 601 (2002).

[44] G. Strinati, Phys. Rev. Lett. **49**, 1519 (1982).

[45] G. Strinati Phys. Rev. B. **29**, 5718 (1984).

[46] M. Rohlfing and S. G. Louie, Phys. Rev. B. **62**, 4927 (2000).

[47] M. Palummo et al 2004 J. Phys.: Condens. Matter **16**, S4313.

[48] J. Wang, J. Ardelean, Y. Bai, A. Steinhoff, M. Florian, F. Jahnke, X. Xu, M. Kira, J. Hone, and X. Y. Zhu, Sci. Adv. **5**, eaax0145 (2019).

[49] L. Meckbach, T. Stroucken, and S. W. Koch, Appl. Phys. Lett. **112**, 061104 (2018).

[50] C. Klingshirn, Semiconductor Optics 3rd edn (Springer, 2007).

[51]] S. Schmitt-Rink, C. Ell, H. E. Schmidt, and H. Haug, Solid State Commun. **52**, 123-125 (1984).

[52] K. T. Winther and K. S. Thygesen 2D Mater. **4** 025059 (2017).

[53] G. Trnkle, H. Leier, A. Forchel, H. Haug, C. Ell, and G. Weimann, Phys. Rev. Lett. **58**, 419 (1987).

[54] T. L. Reinecke, D. A. Broido, E. Lach, V. Kulakovskii, A. Forchel, and D. Gruetzmacher, Superlattices Microstruct. **7**, 437 (1990).

[55] D. Sun, Y. Rao, G. A. Reider, G. Chen, Y. You, L. Brezin, A. R. Harutyunyan, and T. F. Heinz, Nano Lett. **14** (10), 56255629 (2014).

[56] H. Wang, C. Zhang, and F. Rana, Nano Lett. 2015, **15**, 82048210

[57] D. Sangalli, A. Ferretti, H. Miranda, C. Attaccalite, I. Marri, E. Cannuccia, P. Melo, M. Marsili, F. Paleari, A. Marrazzo, G. Prandini, P. Bonf, M. O. Atambo, F. Affinito, M. Palummo, A. Molina-Snchez, C. Hogan, M. Grning, D. Varsano, and A Marini, J. Phys.: Condens. Matter **31**, 325902 (2019).

[58] E. J. Sie, A. Steinhoff, C. Gies, C. H. Lui, Q. Ma, M. Rosner, G. Scho nhoff, F. Jahnke, T. O. Wehling, Y.-H. Lee, J. Kong, P. Jarillo-Herrero, and N. Gedik, Nano Lett. **17**, 7, 4210- 4216 (2017).